Available online at www.sciencedirect.com
SCIENCE DIRECT®
ELSEVIER
Nuclear Instruments and Methods in Physics Research A 539 (2005) 527–539
NUCLEAR INSTRUMENTS & METHODS IN PHYSICS RESEARCH Section A
www.elsevier.com/locate/nima

ELYSE—A picosecond electron accelerator for pulse radiolysis research

J. Belloni[a,*], H. Monard[a], F. Gobert[a], J.-P. Larbre[a], A. Demarque[a], V. De Waele[a], I. Lampre[a], J.-L. Marignier[a], M. Mostafavi[a], J.C. Bourdon[b], M. Bernard[b], H. Borie[b], T. Garvey[b], B. Jacquemard[b], B. Leblond[b], P. Lepercq[b], M. Omeich[b], M. Roch[b], J. Rodier[b], R. Roux[b]

[a]*Laboratoire de Chimie Physique, UMR CNRS/UPS 8000, Bât. 349, Université Paris-Sud, 91405 Orsay, France*
[b]*Laboratoire de l'Accélérateur Linéaire, IN2P3-CNRS, Université Paris-Sud, B.P. 34, 91898 Orsay, France*

Received 31 August 2004; received in revised form 9 November 2004; accepted 9 November 2004
Available online 8 December 2004

Abstract

Recent years have seen an increasing interest in the use of intense, short pulse electron beams for pulsed radiolysis research. Laser driven photo-cathodes inserted in radio frequency (RF) guns are ideal candidates to provide electron beams for time-resolved spectroscopic observation of very fast chemical reactions. These guns have been developed through accelerator R&D programmes in the field of high brightness sources for other applications (linear colliders, free electron lasers). The Physical Chemistry Laboratory at the University of Paris-Sud has created a Fast Kinetics Centre for experimental pulse radiolysis with picosecond time resolution. At the heart of this new facility is a compact 4–9 MeV electron accelerator, ELYSE, using RF gun technology. It has been designed and built by the Linear Acclerator Laboratory at the University of Paris-Sud. We will describe the construction and commissioning of ELYSE, the first machine of this type in Europe.

Keywords: Radiation chemistry; Picosecond pulse radiolysis; Femtosecond laser; Synchronization jitter; Laser photo-cathode RF gun

1. Introduction

The chemical effects of high-energy X- and γ-rays or particles have been studied [1] since the discovery of these types of radiation at the end of the 19th century. Radiation chemists introduced progressively the assumption of short-lived radical species in order to account for the mechanisms yielding the final products. The advent in 1962 of pulse radiolysis techniques [2,3] using pulsed electron accelerators synchronized with time-resolved spectrophotometry permitted the direct

*Corresponding author.
E-mail address: jacqueline.belloni@lcp.u-psud.fr (J. Belloni).

0168-9002/$ - see front matter © 2004 Elsevier B.V. All rights reserved.
doi:10.1016/j.nima.2004.11.006

identification and reactivity of the transient intermediaries of the reactions. The principle was to deliver in a very short pulse a high irradiation dose in order to get detectable concentrations of the short-lived species and to follow directly their decay during their fast reactions. Since the earliest observation of the hydrated electron with microsecond pulses [2,3], a great deal of data was collected on short-lived charged or neutral radicals [4,5], which enable us to understand not only the processes initiated by an irradiation pulse, but more generally any chemical or biochemical mechanism where they are involved.

However, the time resolution of processes which can be observed is limited by the duration of the pulse by which they are generated. Therefore, these machines have evolved towards still shorter pulses delivered by more powerful facilities associated with the required time resolution of the detection line [6]. In the late 1960s, the series of Febetron models used a Marx-surge generator directly coupled to a high-vacuum field emission tube and delivered electron pulses of 3–50 ns [7]. A 50 ps stroboscopic pulse radiolysis facility was constructed by Hunt at Toronto in 1968. The Cherenkov light simultaneously emitted in air by a train of electron pulses was used for the probe analysis [8]. A similar system was developed at Hokkaido University [9]. The generation of single picosecond electron pulse was used in the Argonne National Laboratory in 1975 for the construction of a pulse radiolysis facility with 50–100 ps time resolution [10]. A 35 MeV electron linear accelerator with pulses of 18 ps at half-height was then installed at the University of Tokyo, Tokaï-Mura [11].

A new generation of subpico- and picosecond electron accelerators has appeared in the last decade, which use powerful UV laser pulses triggering a photo-cathode to produce the initial electron bunch. Such photo-cathode RF guns were developed for pulse radiolysis facilities at Brookhaven National Laboratory [12,13], at Nuclear Engineering Research Laboratory, Tokaï-Mura [14,15], at Osaka University [16], at the University of Paris-Sud [17,18], at Sumitomo Heavy Industries [19] and at Waseda University [20].

The ELYSE facility at the University of Paris-Sud [21] aims to provide the French physical chemistry community with a facility for the study of fast chemical reaction dynamics. ELYSE is named after Lysis (Greek for degradation) by Electrons. This Fast Kinetics Centre at Orsay is based around a femtosecond laser facility used for triggering the photo-cathode and a picosecond electron accelerator used for pulse radiolysis experiments. The combination of laser and electron beams will allow the physical chemistry community to perform pump–probe experiments with high time resolution. Irradiation of chemical samples will be possible with both electron beams (pulse radiolysis) or laser beams (also used independently for ultra-fast photochemistry). The Linear Accelerator Laboratory had the responsibility for the design and construction of the electron accelerator for the radiolysis experiments. Our design has benefited from the experience we have gained with the RF gun project, CANDELA [22].

This paper will be concerned with the ELYSE electron accelerator facility. We will concentrate on the description of the design of the hardware, which was built in order to fulfill the requirements summarized in Table 1, and on the first tests which were performed using the electron beam.

2. Design of the pulse radiolysis instrument

The desired beam characteristics from ELYSE are shown in Table 1. To obtain these characteristics, we have chosen to employ an RF gun with a photo-cathode. The photo-cathode is triggered by a 263 nm laser pulse obtained from the frequency tripled 790 nm photolysis laser. The use of the laser makes a photo-cathode an ideal choice of electron source as precise synchronization, using a 79.8 MHz quartz oscillator controlling both the pump laser beam and the klystron RF of the laser-triggered electron beam should be possible. Moreover, a small fraction of the laser beam will be deviated to produce a pulsed white light source to be used as a synchronized probe light for the spectro-photometric detection of the transients. The ELYSE facility is shown schematically in

Fig. 1 along with the areas used for ultra-fast photolysis and pulse radiolysis, the latter being surrounded by radiation shielding.

2.1. Laser equipment

The disposition of the existing building which was renovated to house ELYSE, was such that the ideal place to install the laser was on the ground floor, vertically above the shielded target room in the basement where the electron gun was installed. The femtosecond laser chain is based on a commercial system (Spectra Physics) (Fig. 2). The cavity length of a Ti:Sapphire oscillator is adjusted to be synchronized with the 79.8 MHz frequency of the quartz master-oscillator which also controls the accelerator timing. Ultra-short pulses of 90 fs are delivered at 790 nm. The energy of the pulses at this stage is only about 10 nJ. They are therefore amplified by a regenerative amplifier using the chirped pulse amplification (CPA) technique. At the output, the (790 nm, 100 fs) pulses have an energy of 1.1 mJ. The laser source is unique in as far as, just before the laser pulse compression, a fraction of 1–50 pulses from the 1000 per second (1 kHz) are separated by a Pockels cell and Glan–Taylor polarizer system defining the repetition rate. Both pulses, which are produced in parallel at 790 nm, (and 1.1 mJ) are compressed differently. Those used to excite the accelerator photo-cathode (1–50 Hz) were of 2 ps and more recently of 120 fs, whereas the others used independently for femtochemistry studies (999–950 Hz) are ultra-short, 100 fs at 790 nm [23–25].

Table 1
Requirements of the ELYSE pulsed electron accelerator

Beam energy (MeV)	4–9
Pulse duration (FWHM) (ps)	<5
Charge per pulse (nC)	>1
Energy spread (RMS)	<2.5%
Normalized emittance (RMS) (mm-mrad)	<60

The laser beam at 1–50 Hz is then transferred down through a hole in the concrete and lead shielding between the laser and the accelerator rooms, its frequency is tripled to 263.3 nm and transported to the photo-cathode. The energy per pulse at 263 nm is up to 20 μJ. In order to obtain normal incidence of the laser beam onto the photo-cathode, and thus to produce photo-electrons with a time structure as close as possible to

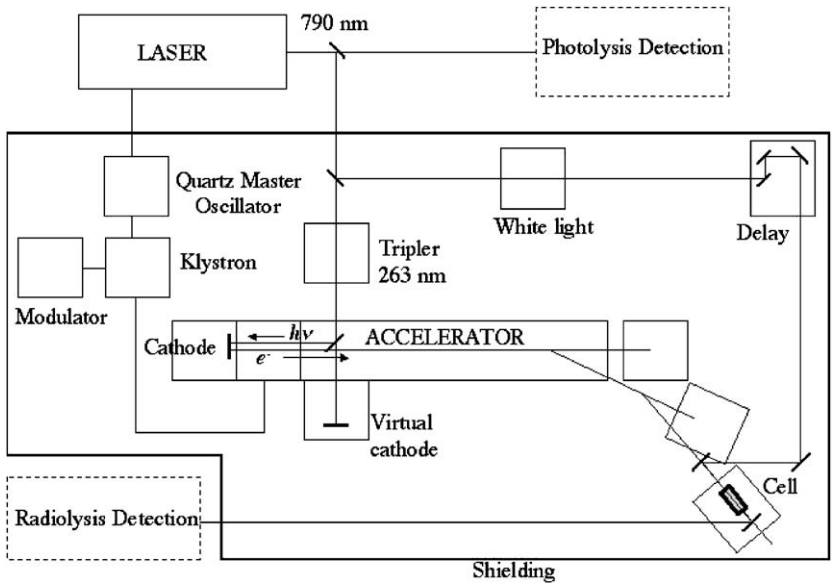

Fig. 1. Principle of the laser driven RF electron accelerator.

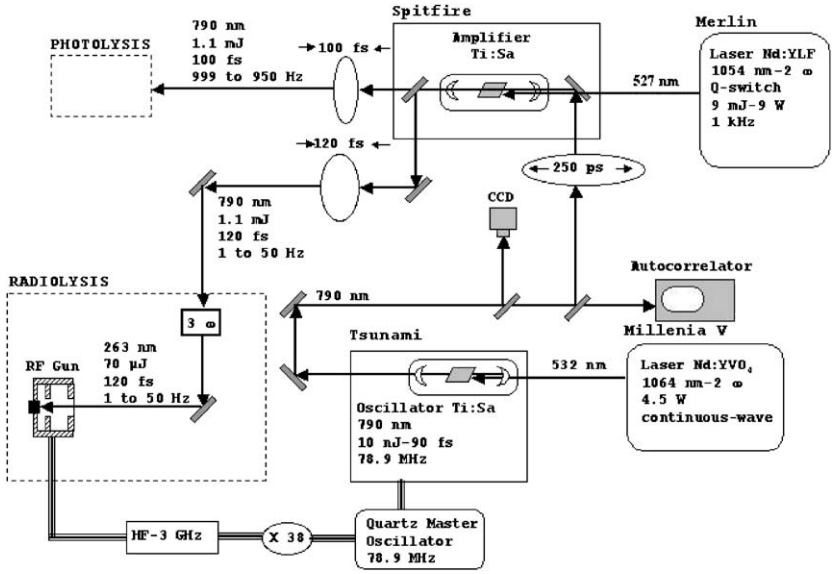

Fig. 2. A schematic of the ELYSE laser chain.

that of the laser, the beam, which is injected into the vacuum gun chamber through a transparent window, is reflected almost perpendicularly onto the cathode by a laser entrance mirror (LME) (Figs. 1 and 4). The mirror is in fact slightly shifted relative to the electron beam axis so as to prevent irradiation. The laser pulse energy delivered to the photo-cathode is measured, after reflection by a switch-able laser exit mirror (LMEx), on a virtual cathode (VC) (Figs. 3 and 4), which is located on a side line perpendicular to the main gun axis and equipped in situ with a Joulemeter.

2.2. The photo-cathode and vacuum preparation chamber

The extractable photo-charge from the cathode, Q in nC, is given by

$$Q = 2.1 \times E_\lambda \times \eta, \quad (1)$$

where E_λ (in μJ) is the laser pulse energy at the wavelength $\lambda = 263\,\text{nm}$ and η is the quantum efficiency of the photo-cathode (in %).

The nominal beam requirements for ELYSE were a total photo-charge of $\geqslant 1\,\text{nC}$ and a pulse duration of $\leqslant 5\,\text{ps}$ FWHM for the 60° deviated beam line (Fig. 3). However, there is also a strong scientific interest in obtaining bunch charges of ~10 nC. The need to extract such high charges with microJoule laser pulses (Eq. (1)) requires the use of Cs_2Te photo-cathodes which are presently considered to be the best choice for high quantum efficiency ($\eta \approx 1\%$ e^- per 263 nm photon) [26] and acceptable lifetime. Since the Cs_2Te coating is sensitive to oxidation by air, it should be prepared in situ under extremely low-pressure conditions. A vacuum chamber based on the chamber used at CERN/CTF [26] and dedicated to Cs_2Te preparation was built for this purpose (Fig. 4).

Vapours of caesium and tellurium are obtained by melting and evaporation of solid Cs chromate and Te under vacuum, using an electric resistor located in each crucible (Fig. 4). Both are fixed on a mobile arm. After pre-heating the crucibles for out-gassing and residual gas analysis, the Te crucible is translated in front of the cathode protected by a mask. The cathode support (Fig. 4) is heated up to 120°C by auxiliary resistors and temporarily masked until the evaporation/condensation rate is stabilized. A quartz micro-balance (Fig. 4) is located close to the cathode and is used to check the stabilization and then to determine the rate of deposition first of Te, then of Cs, and to set the duration of each deposition. The

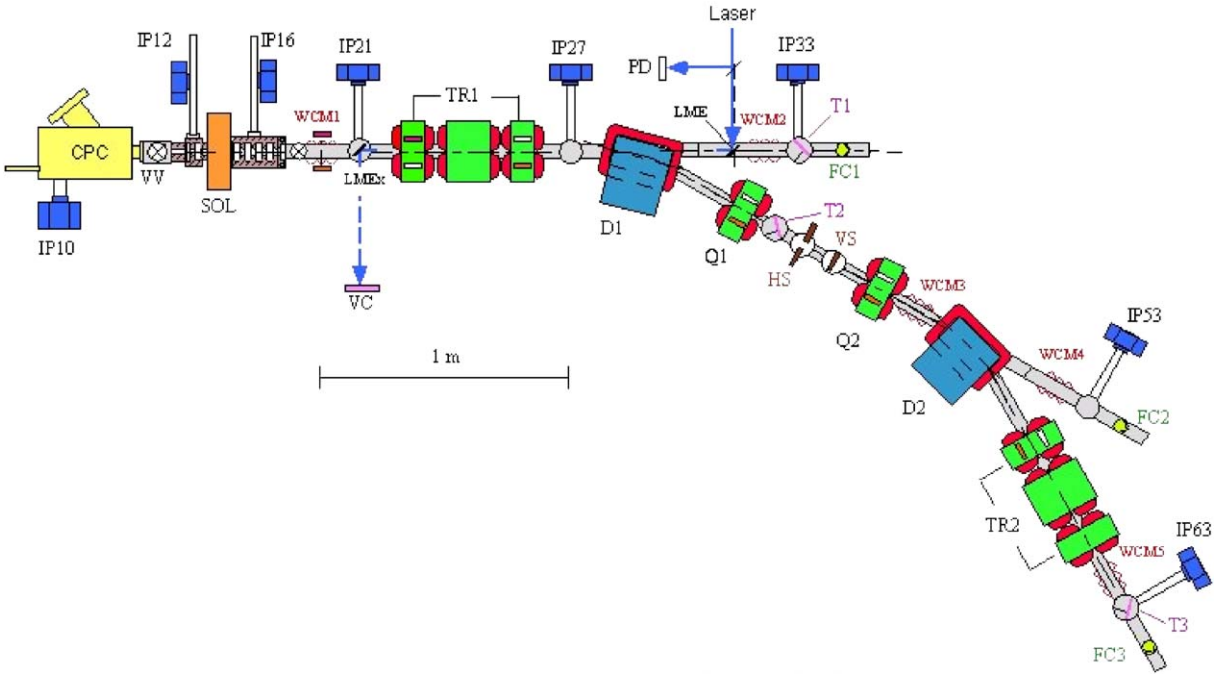

Fig. 3. A general schematic of the ELYSE accelerator. IP: ion vacuum pump; CPC: cathode preparation chamber; VV: vacuum valve; SOL: solenoid; D: dipole; TR1 and 2: triplets; Q: quadrupole; WCM: wall current monitor; FC: Faraday cup; PIQ: Ion pump; T: translator for Cherenkov light emitter and visualization screen; LME: laser entrance mirror; LMEx: laser exit mirror; VC: virtual cathode; HS: horizontal slit; VS: vertical slit.

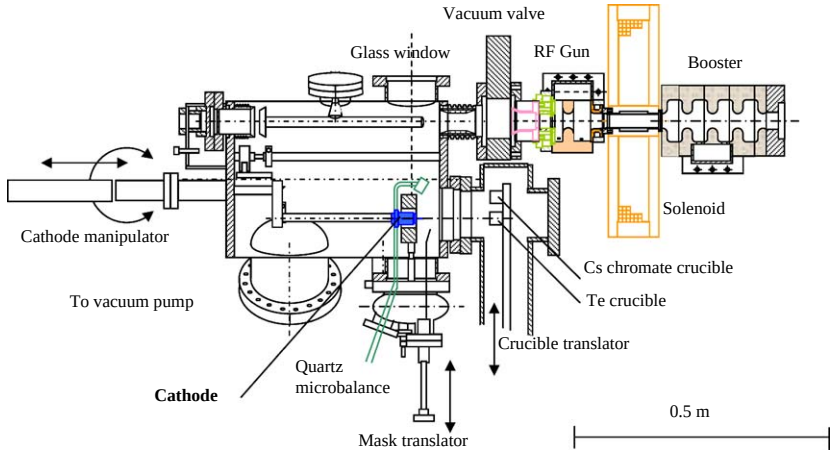

Fig. 4. Horizontal section through the vacuum chamber for the Cs_2Te photo-cathode preparation.

rate of condensation is first stabilized at about 0.3 nm/s before exposing the cathode to condensation. The external mask is then removed from the cathode still protected by a circular mask (internal diameter 19 mm). Condensation of Te lasts typically during 5 min up to a depth of 20 nm and is

stopped by the interposition of the mask. The operation is repeated for Cs deposition after translating the Cs chromate crucible heated at 800 °C in front of the cathode, then stabilizing the Cs evaporation rate as controlled by the quartz microbalance and finally removing the mask. After 40 min of deposition, the thickness of the Cs coating is 16 nm. The Cs_2Te compound is formed by diffusion of Cs into the Te coating [27]. Again, the cathode mask is used to stop the deposition up to the cooling and removing of the crucibles using the translator. The Cs_2Te photo-cathode position is then adjusted through manipulation of the arm on the axis of the gun cavity (Fig. 4). The appearance of the photo-cathode after preparation and during its lifetime may be visualized directly through the glass window of the chamber. The photo-cathode preparation chamber is connected to the accelerator cavity by a vacuum valve (VV) (Fig. 3), which allows one to isolate the chamber from the gun.

2.3. The RF gun and booster

As shown in Table 1, the energy of the ELYSE beam should be variable in the range of 4–9 MeV. The electron gun is a 1-1/2 cell, 3 GHz structure based essentially on the CLIC Test Facility (CTF) gun which has produced high bunch charges using Cs_2Te cathodes [28–30]. This gun provides a beam of 4 MeV for an input power of 8.3 MW. The additional acceleration to reach 9 MeV is provided by a four-cell booster cavity which is identical to that used on CTF. Nevertheless, we have made slight modifications to allow operation of the gun at lower cathode gradients (65 MV/m) with the aim of reducing the dark current while still allowing transport of the high charge through the booster. Optimization of the gun was performed with the simulation code SUPERFISH [31]. In order to allow the intense beam to propagate cleanly through the booster, there is a water-cooled solenoid between the two RF structures (Fig. 4). The magnetic field distribution was used as input for PARMELA [32] code calculations of the electron beam envelope. The magnetic field of the solenoid was calculated using the code POISSON [31].

2.4. The RF distribution system

The RF power for the gun and booster is provided by a TH2130 klystron (Thomson-CSF, 20 MW, 4 ms) and a purpose built modulator. The RF network is designed to allow variable energy operation of the linac. The power from the klystron passes through a four-port ferrite circulator and is then divided into two branches by a 3 dB power splitter. The first branch is connected to the RF gun. The second branch is connected to the booster section and includes a variable attenuator, to adjust the energy gain from the booster, and an adjustable phase-shifter, to vary the booster phase with respect to the phase of the RF gun. RF pickups allows one to measure the RF field in the gun and the booster.

2.5. The transport line

After acceleration to the desired energy, the beam can be transported to any one of three experimental areas (EA). EA-1 is directly downstream of the accelerating section whereas EA-2 and EA-3 are at 30° and 60°, respectively, to EA-1 (Fig. 3). The beam is deviated to EA-2 or 3 with the use of rectangular C-type dipole magnets (bend angle = 30°, bend radius = 500 mm). The main windings were calculated to produce a maximum magnetic field of 0.1 T. A secondary winding allows one to cancel residual fields of the order of 20 G, in order to deliver the beam to experimental areas EA-1 and 2 when required. Transverse focusing is assured by quadrupole triplets up and downstream of the dipole pair as well as a pair of quadrupoles between the two dipoles. The design and calculated settings of the transport line were made bearing in mind that the most important parameter, for the experimental targets, is the bunch length. The layout of the line is rather classical. The beam exiting the booster encounters a first quadrupole triplet followed by two dipoles with a pair of quadrupoles between them and, finally, a second triplet (Figs. 3 and 4). The EA-3 transport line has a point of symmetry centred between the pair of quadrupoles. This means that the pairs of dipoles, quadrupoles and triplets

are identical as are the lengths of the corresponding drift spaces.

The RMS beam parameters at the exit of the booster, calculated using PARMELA, were used to provide input Twiss parameters for TRACE-3d [33] in each of the phase spaces (x, x'), (y, y') and (phase, energy). TRACE-3d has the advantage of allowing quadrupole fitting procedures and permits one to quickly check on the transport. On the other hand, only the linear part of the space charge field is taken into account. For this reason, we used PARMELA to calculate the envelope through the entire transport lines with the quadrupole settings found using TRACE-3d. No major discrepancies are seen when comparing the transverse RMS beam envelopes. However, the final bunch length calculated with PARMELA appears to be slightly longer than that calculated with TRACE-3d. The difference may be due to the inclusion of the non-linear space charge fields when using PARMELA.

Now let us discuss the transport setting from the exit of the booster up to the experimental area EA-3. The phase space co-ordinates at the exit of the transport line, x_i, are related to those at the entrance, x_{0j}, by the transfer matrix R_{ij} using the equation

$$X_i = \sum_{j=1}^{6} R_{ij} x_{0j} \quad (i = 1, 2, \ldots, 6), \tag{2}$$

where $x_i \equiv (x, x', y, y', \mathrm{d}z, \mathrm{d}p/p)$. First, we find the correct settings for the pair of quadrupoles (Q4 and Q5) in order to have the transport matrix elements $R_{51} = R_{52} = 0$. This setting makes any bunch compression independent of the geometric terms at the exit of the booster cavity. Moreover, it is also the correct setting for a first-order achromatic transport (neglecting space charge effects). The fields of the first triplet are then adjusted to give a reasonable value for the horizontal beam size between the two dipoles. Finally, the second triplet is set to deliver the required beam size, at EA-3. It is then necessary to re-adjust Q4 and Q5 to maintain $R_{51} = R_{52} = 0$. If the gun and booster are adjusted to provide the required phase-energy correlation then bunch length compression occurs after the beam traverses the two dipoles.

The intensity and position of the beam is observed upstream of each EA by a wall current monitor (WCM) and a Faraday cup (FC). Ceramic screens are used to indicate the transverse beam profile. The bunch length is measured from the pulse length of Cherenkov light, which is emitted by sapphire screens and transferred through the mirrors of an optical line to the detection room. There, the light pulse is measured using a streak camera [34]. An adjustable, and moveable, horizontal slit (HS) placed at a distance, $L = 800$ mm, downstream of the first dipole exit face gives some indication of the beam energy spread by measuring the horizontal beam profile (Fig. 5). A system of five ion pumps distributed along the transport line maintains the required vacuum level for the machine ($\approx 2 \times 10^{-9}$ mbar).

2.6. Accelerator control systems

The control systems of the accelerator consist of one acquisition PC (industrial PC IAC), keeping track of the control parameters coming from the electronic racks, and one supervision PC used by the operator for turning the machine on, and setting the beam. The software controlling the accelerator was realized by EuroMev with the National Instrument software LabVIEW®.

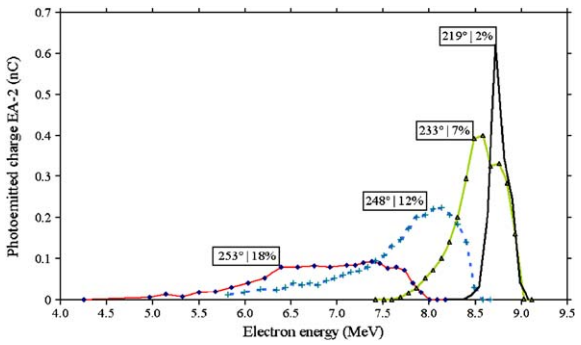

Fig. 5. Energy spectra of the electron beam at EA-2. For each spectrum the values of the phase and of $\delta E/E$ are shown. Laser pulse energy: 4 μJ, HS: 5 mm, VS: 25 mm.The spectrum is obtained by scanning D1. Maximum charge at EA-1 (253°): 2.5 nC. The minimum value of $\delta E/E$ is 2% at half-height for 8.8 MeV.This optimization is obtained by decreasing the phase 34° from the setting that yields the maximum charge at EA-1 (253°).

The communication between the two PCs uses the TCP/IP protocol.

Concerning the RF, the operator has control of different parameters: the level of power going towards the RF gun using the klystron high voltage (7–13 kV), the level of power (0–6 MW) going towards the booster using an RF attenuator, the gun-booster relative phase, the width and delay of the RF macropulse, the working temperature of the gun and of the booster (independently, with $a \pm 0.1\,^{\circ}C$ accuracy). The software enables us to control and monitor all of the magnet power supplies for the beam transport (the solenoid, two bending dipoles, four horizontal and vertical steering dipoles, eight quadrupoles). Settings for typical shots at 9 MeV or 5 MeV can be saved and automatically restored.

Concerning the beam diagnostics, electric translators are used for imaging the beam with alumina screens, or for positioning the sapphire radiators used in the Cherenkov bunch length measurement. The software allows one to translate those elements automatically to the ''screen'' or ''Cherenkov'' position. Pneumatic actuators are used for the Faraday cup translation movement which allows us to measure the beam charge and to stop the beam, when needed, just before the exit windows.

The software displays pressure readings from the different ionization gauges and ion pumps located along the beam line. The software also enables us to send a synchronized signal to the experimental detection room, with a width and a delay adjustable by the operator.

For safety requirements, the turning on of the gun is interlocked to the contacts of closing the concrete and lead doors and to an upper dose level inside the irradiation room. It is also controlled by suitable vacuum level in the gun and coolant flow of the machine when running.

Oscilloscopes permit the operator to check different information such as the signals of the RF gun reflected power, the electric field level in the cavities, the series of WCM signals, etc. The operator can also check the laser spot on the virtual cathode, and move the direction of the laser beam to the cathode with an automated mirror.

3. Pulsed beam properties

3.1. Uncoated metal photo-cathode

Following a period of conditioning of the RF distribution system, the RF gun and booster section (first at 5 Hz and then 10 Hz), a first attempt was made to produce a beam using a polished, uncoated, copper cathode. Fig. 6 shows the RF filling of the cavity, the laser pulse (which is applied during the plateau of the RF pulse and measured using a photo-diode), the photo-current signal produced by the laser pulse measured at EA-1 by the WCM (with an apparent large width due to the electronic response time) and by the Faraday cup. Fig. 6 clearly shows that the photo-current signal is superimposed on the dark current signal. The incident RF power to the gun, P_{gun} is 5.2 MW ($E_{acc} = 70$ MV/m). During conditioning, dark current was detectable for gradients starting from 33 MV/m. As the quantum efficiency of the copper cathode is low and ranges from 10^{-4} to 2×10^{-6} [35,36], the maximum charge extracted by photo-emission is only ~400 pC (for a laser energy on the cathode of 20 μJ). This does not indicate a true measure of the quantum efficiency since it is the charge measured at EA-1: dark current electrons may be lost while passing through the RF cavities and the magnets.

After several days of operation at a repetition rate of 25 Hz and then 50 Hz, we observed a dramatic increase in the level of the dark current signal and a strong increase in the temperature of the tuning plunger in the first (half) cell of the RF gun. In addition, the resonant frequency of the gun changed to a higher value. After modifying the position of the tuner, its temperature during operation was reduced and the cavity's resonant frequency restored to its normal value. However, this had no effect on the dark current which remained abnormally high: 80 nC per pulse for a 9 MeV beam conditions measured at EA-1 with a specific optics setting. This increased dark current was still present even when the repetition rate was reduced again to 10 Hz. The need to lower the dark current led us to bake out the RF gun and booster simultaneously for a 2 week period, at 150 °C. This decreased the dark charge by a factor of 2.5. Dark

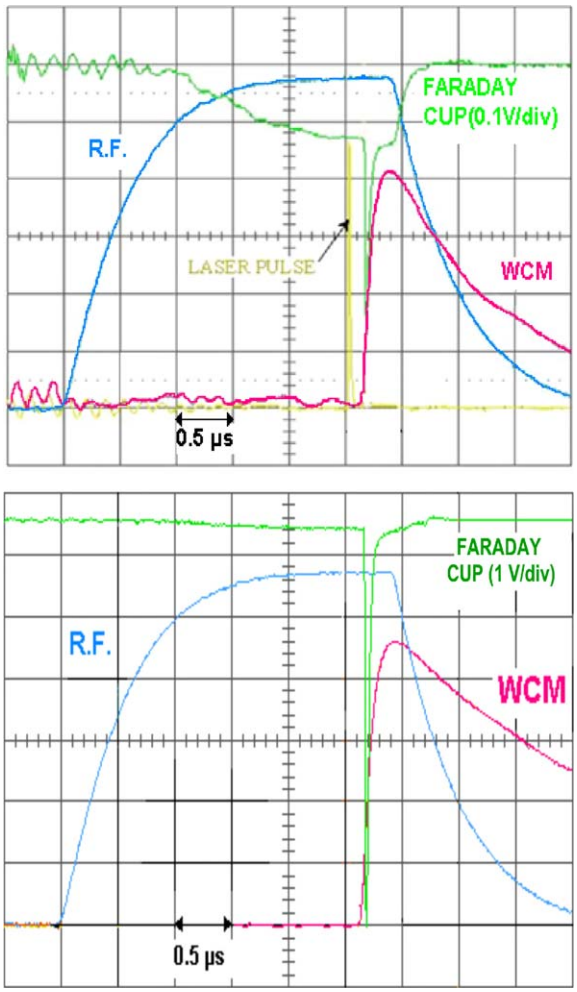

Fig. 6. Oscillograms showing (left to right): the RF filling of the gun, the laser pulse and the electron pulse. Top: Signals with Cu photo-cathode (the electron pulse is composed of the dark current and the photo-current). Bottom: Signals with Cs_2Te photo-cathode (the dark current is now negligible compared to the photo-current).

current can be due to electron field emission from microscopic irregularities on the copper surface or the presence of tiny "polluting" elements inside the cavity. Increased electron losses at high repetition rate may have been responsible for desorption of pollutants within the copper surface leading to the increased dark current. The bake-out would have reduced the presence of adsorbed gases on the cavity. Experience at several laboratories now indicates that extreme care in the preparation and installation of RF guns is needed to minimize dark current (high-pressure rinsing with ultra-clean water, installation under laminar flow of clean air, etc.), precautions which were not taken with the installation of the ELYSE gun. However, the operation of RF guns in high electric fields means that some level of dark current will always be present.

Although the bake-out helped to reduce the dark current, we can still observe a 30 nC dark charge per pulse (for specific settings of the quadrupoles and the solenoid) for 9 MeV beam conditions. Changing the optics allows us to reduce this dark current, especially by adjusting the solenoid field in between the RF gun and the booster. Moreover, the dark current has a very broad energy spectrum and so the first dipole reduces the dark current delivered to EA-3 since this magnet is selective in energy. The HS can also be adjusted in width to reduce the dark current. The combined effect of these elements allows us to obtain an acceptable ratio between the dark charge and the photo-emitted charge at EA-3 of typically 2%.

3.2. Cs_2Te Photo-cathode

The photo-current extracted from the Cs_2Te photo-cathode is 1–5 nC. Therefore, the dark current becomes a negligible part of the total current, as shown in Fig. 6 (note that the detection sensitivity is 10 times less for Cs_2Te than for Cu). When the cathode is freshly prepared, the current is somewhat larger. The variation of the photo-current as a function of the photo-cathode ageing is presented in Fig. 7 along with the energy of the 263 nm laser pulse, measured on the virtual photo-cathode. During this period of 18 accumulated days of use over around 1 year, the geometry of the laser spot on the cathode was constant (5 mm diameter) and other adjustments of the accelerator were unchanged except the energy of electrons which was generally 9 MeV and, in some experiments, 5 MeV. Independent of the fluctuations from day to day of the laser pulse energy, and of the structure of the laser beam, the photo-current increases roughly with the laser pulse energy. The current emitted by the photo-cathode during

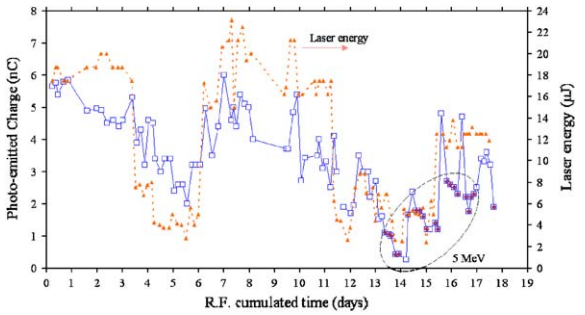

Fig. 7. Cs_2Te photo-cathode response as a function of laser pulse energy and cathode age over 1 year. Laser pulse energy (▲). Electron energy: 9 MeV (□), 5 MeV (■). HF phase and triplets optimized. Diameter of the laser spot on the cathode: 5 mm.

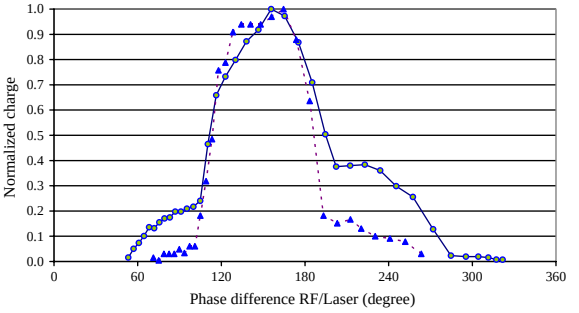

Fig. 8. Dependence on the phase difference between the RF and the laser pulses of the photo-charge per pulse. Direct beam exit EA-1. Photo-charge normalized relative to the optimized charge of 5 nC. Laser pulse energies of 1 μJ (▲) and 15 μJ (◇) (spot diameter 5 mm).

ageing over 1 year of running is remarkably stable. In the absence of any leak in the chamber, the Cs_2Te deposit is particularly strong and does not need to be prepared too often.

The dependence on the phase difference between the RF and the laser pulses of the photo-charge per pulse, which is measured at the direct beam exit EA-1 and normalized relative to the optimized charge of 5 nC, is shown in Fig. 8 for two values of the laser pulse energy, 1 and 15 μJ (spot diameter 5 mm). According to simulations, the main band of the photo-charge extends over 100° of phase difference. However, the peak is superimposed to an unusually broad component starting from 50° and extending with a high intensity to 280° (instead of over a half RF period, that is 180°), particularly when the laser pulse energy increases. Studies are in progress to account for these results.

The photo-current intensity depends, at a fixed laser pulse energy (about 15 μJ), on the size of the laser beam spot onto the cathode, as shown in Fig. 9. The equivalent radius corresponds to that of an ideal circular spot of the same area as the measured area of the real spot. Indeed, the higher the spot size and the lower the density of photons, the lower is the probability of electron-hole pair loss by recombination in the semiconductor. Currents as high as 7.5 nC have been measured at the beam exit EA-1 for an equivalent spot diameter of 15 mm. However, the pulse width also increases up to about 15 ps. The dependence of the

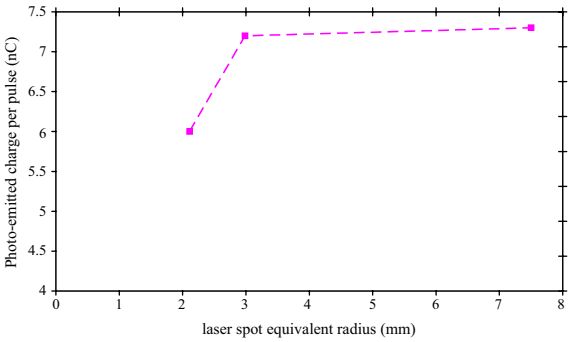

Fig. 9. Dependence of the electron pulse current on the laser spot diameter.

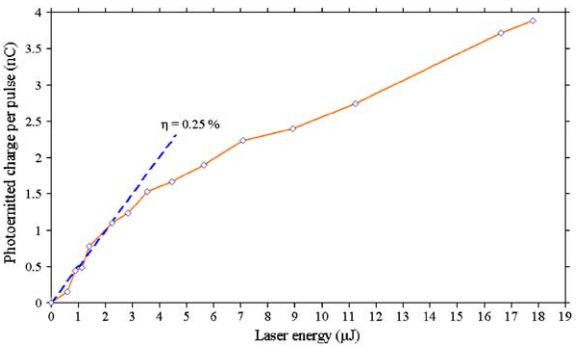

Fig. 10. Dependence of the electron pulse charge on the laser pulse energy at the beam exit EA-1 (Laser beam diameter on the cathode: 8 mm, electron energy: 9 MeV).

current on the laser pulse energy up to 18 μJ, measured within the same day under other identical conditions, is shown in Fig. 10. The

photo-current is linear in the lower energy range with a slope of $\eta = 0.25\%$. Beyond 4 μJ, the quantum efficiency starts to decrease.

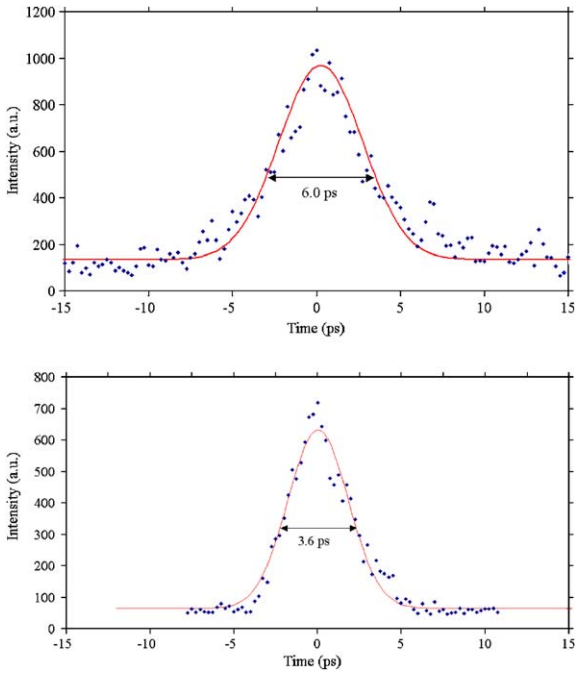

Fig 11. Time-resolved photo-current signals with the Cs_2Te photo-cathode. Pulse duration measured using Cherenkov light and the streak camera. Top: Direct beam EA-1. Bottom: Deviated beam EA-3.

Fig. 11 shows streak camera images obtained from Cherenkov radiation from the electron pulses obtained on the direct line EA-1 and the deviated line EA-3 with the Cs_2Te coated photo-cathode prepared in situ in the vacuum chamber. The pulse width for 9 MeV electrons is 6 and 3.6 ps, respectively.

The shape of the beam cross-section close to the exit windows of the accelerator may be visualized by the spot of the brown colour due to F-centres formed in the depth of a standard glass slide (Fig. 12). Presently, this type of detection is used systematically before each series of irradiation experiments. Under optimized conditions, the spot is of circular symmetry. The densitometric analysis of the spot indicates the relative distribution of the dose absorbed along the spot diameter in Fig. 12 for 9 MeV electron pulses on the deviated line EA-3.

4. Conclusion

The ELYSE accelerator has produced, at a repetition frequency of 25 Hz, a few nC, 6 ps-pulses of 9 MeV electrons for the direct line EA-1 and pulses of a few nC, 3.6 ps pulses, 9 MeV, for the deviated line EA-3, using a Cs_2Te photo-cathode prepared in situ in a vacuum chamber. The response of the cathode is particularly stable

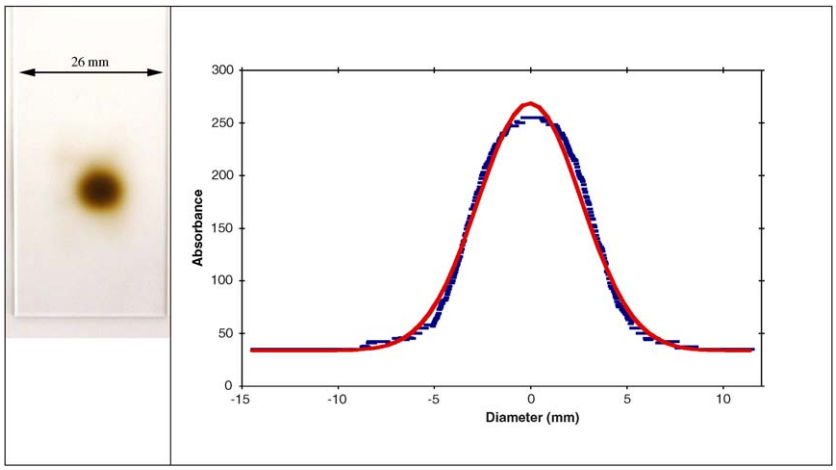

Fig. 12. Dose profile delivered by the 9 MeV electron beam on a glass slide close to the exit window of EA-3. Accumulation of 2600 pulses. Left: irradiation spot. Right: densitometric profile.

when ageing. The ratio of dark current to photocurrent is less than 2% at 5 and 9 MeV for the direct line EA-1 and the deviated line EA-3, respectively.

Acknowledgements

We are particularly indebted to Professor Alain Fuchs, Head of the Laboratoire de Chimie Physique, for his continuous encouragements during the realization of this project.

We acknowledge the assistance of personnel from LURE, especially M. Corlier and J. Vétéran, for their help in specifying and testing the magnets, M. Begard and P. Corona for the construction of the magnet power supplies, J.C Frank and M. Geeraert for assistance in matters concerning radiation security and P. Robert for the design of the cavity cooling system. We thank also the technical support of LAL personnel, especially G. Arnaud, F. Blot, J.N. Cayla, V. Chaumat, F. Cordillot and J. Lamouroux.

The construction of the ELYSE facility, the accelerator, the femtosecond laser equipment, and the office building has been supported by the Université of Paris-Sud, the Chemical Sciences Department of CNRS, the Ministry of National Education, Research and Technology, the Conseil Régional de l'Ile-de-France and the Conseil Général de l'Essonne.

References

[1] J. Belloni, M. Mostafavi, J. Chim. Phys. (2000) 11.
[2] J.W. Boag, E.J. Hart, Nature 197 (1963) 45.
[3] J.P. Keene, Nature 197 (1963) 47.
[4] G. Buxton, C.L. Greenstock, W.P. Helman, A.B. Ross, J. Phys. Chem. Data 17 (1988) 513.
[5] P. Wardman, J. Phys. Chem. Data 18 (1989) 1637.
[6] L.K. Patterson, in: Farhataziz, M.A.J. Rodgers (Eds.), Radiation Chemistry. Principles and Applications,, VCH, Weinheim, 1987 65p.
[7] F.M. Charbonnier, J.P. Barbour, J. L. Brewster, in: G.E. Adams, E.M. Fielden, B.D. Michael, (Eds.), Fast Processes in Radiation Chemistry and Biology, The Institute of Physics and John Wiley (1975) 3.
[8] M.J. Bronskill, W.B. Taylor, R.K. Wolff, J.W. Hunt, Rev. Sci. Instr. 41 (1970) 333.
[9] T. Sumiyoshi, M. Katayama, Chem. Lett. (1982) 1887.
[10] C.D. Jonah, M.S. Matheson, J.R. Miller, E.J. Hart, J. Phys. Chem. 80 (1976) 1267.
[11] H. Kobayashi, T. Ueda, T. Kobayashi, M. Washio, S. Tagawa, Y. Tabata, Nucl. Sci. Instr. 179 (1981) 223.
[12] J.F. Wishart, in: C.D. Jonah, B.S.M. Rao (Eds.), Radiation Chemistry: Present Status and Future Trends, Studies in Physical and Theoretical Chemistry, vol. 87, Elsevier Science, Amsterdam, 2001, p. 21 (Chapter 2)
J.F. Wishart, A.R. Cook; J.R. Miller, Nucl. Instr. and Meth. Phys. Res. A, 2004, in press.
[13] J.F. Wishart, in: J.F. Wishart, D.G. Nocera (Eds.), Photochemistry and Radiochemistry; Adv. Chem. Ser. 254 (1998) 35.
[14] Y. Muroya, T. Watanabe, G. Wu, X. Li, T. Kobayashi, J. Sugahara, T. Ueda, K. Yoshii, M. Uesaka, Y. Katsumura, Radiat. Phys. Chem. 60 (2001) 307.
[15] Y. Muroya, M. Lin, T. Watanabe, G. Wu, T. Kobayashi, K. Yoshii, T. Ueda, M. Uesaka, Y. Katsumura, Nucl. Instr. and Meth. Phys. Res. A 489 (2002) 554.
[16] T. Kozawa, Y. Misutani, K. Yokoyama, S. Okuda, Y. Yoshida, S. Tagawa, Nucl. Sci. Instr. A 429 (1999) 471.
[17] J. Belloni, J.-L. Marignier, M. Gaillard, Cahiers Radiobiol 8 (1998) 25.
[18] J.C. Bourdon, T. Garvey, J. Le Duff, M. Gaillard, Proceedings of the 19th International Linear Accelerator Conference, Chicago, 1998, 645p.
[19] Y. Aoki, J.F. Yang, M. Hirose, F. Sakai, A. Tsunemi, M. Yorozu, Y. Okada, A. Endo, X.J. Wang, I. Ben-Zvi, Nucl. Sci. Instr. Meth. A 455 (2000) 99.
[20] M. Washio, Y. Hama S. Kashiwagi, R. Kuroda, T. Kobuki, T. Hirose, Ind. Soc. Rad. Photochem. (2000) 280.
[21] J. Belloni, M. Gaillard, H. Monard, M. Mostafavi, I. Lampre, H. Remita, J.L. Marignier, J.C. Bourdon, T. Garvey, Proc. UVX 2002, J. Phys. IV France 108 (2003) 243.
[22] C. Travier, G. Devanz, B. Leblond, B. Mouton, Nucl. Instr. and Meth. Phys. Res. A 393 (1997) 451.
[23] R. Krolicki, W. Jarzeba, M. Mostafavi, I. Lampre, J. Phys. Chem. A 106 (2002) 1708.
[24] B. Soroushian, I. Lampre, S. Pommeret, M. Mostafavi, in: M. Martin, C. Hynes (Eds.), Femtochemistry and Femtobiology: Ultrafast Events in Molecular Science, vol. 6, 2004. p. 241.
[25] H. Kang, C. Dedonder-Lardeux, C. Jouvet, S. Martrenchard, G. Grégoire, C. Desfrançois, J.-P. Scherman, M. Barat, J.A. Fayeton, Phys. Chem. Chem. Phys. 6 (2004) 26.
[26] E. Chevallay, J. Durand, S. Hutchins, G. Suberlucq, H. Trautner, Proceedings of the 19th International Linear Accelerator Conference (Chicago), 1998;
E. Chevallay, J. Durand, S. Hutchins, G. Suberlucq, M. Wurgel, Nucl. Instr. and Meth. Phys. Res. A 340 (1994) 146.
[27] A. di Bona, F. Sabary, S. Valeri, P. Michelato, D. Sertore, G. Suberlucq, J. Appl. Phys. 80 (1996) 3024.

[28] R. Bossart, et al., Nucl. Inst. and Meth. Phys. Res. A 340 (1994) 157.
[29] H. Monard, J.C. Bourdon, J. Le Duff, T. Garvey, B. Mouton, J. Rodier, Y. Thiery, M. Gaillard, Particle Accelerator Conference (New York), (1999) 2012.
[30] T. Garvey, M. Bernard, H. Borie, J.C. Bourdon, B. Jacquemard, B. Leblond, P. Lepercq, M. Omeich, M. Roch, J. Rodier, R. Roux, F. Gobert, H. Monard., Proc. Eur. Accelerator Conference (2002) 254.
[31] J.H. Billen, L.M. Young, Poisson Superfish, Los Alamos Nat. Lab., Report LA-UR-96-1834.
[32] L. Young, J. Billen, The particle tracking code PARMELA, Proceedings of the Particle Accelerator Conference, 2003, p. 3521.
[33] K.R. Crandall, D.P. Rustoi, Trace3-D documentation, Los Alamos Nat. Lab., Report LA-11054-MS, 1987.
[34] M. Geitz, S. Schreiber, G. Von Walter, D. Sertore, M. Bernard, B. Leblond, 21st FEL Conference, vol. 2, 1999, II, p. 83.
[35] T. Srinivasan-Rao, J. Fischer, T. Tsang, J. App. Phys. (1991) 69.
[36] E. Chevallay, J. Durand, S. Hutchins, G. Suberlucq, M. Wurgel, Nucl. Instr. and Meth. Phys. Res. A 340 (1994) 146.